Investigating the Vertical Structure of Interactions between Radiation, Circulation and Moisture in Tropical Cyclones

Bosong Zhang[1,2*,3*], Brian J. Soden[1]

1. Rosenstiel School of Marine and Atmospheric Science, University of Miami, Miami, Florida

2. Program in Atmospheric and Oceanic Sciences, Princeton University, Princeton, NJ

3. NOAA/Geophysical Fluid Dynamics Laboratory, Princeton, NJ

Gabriel A. Vecchi[4, 5]

4. Department of Geosciences, Princeton University, Princeton, NJ

5. High Meadows Environmental Institute, Princeton University, Princeton, NJ

To be submitted to *JAMES*

2021

Corresponding author: Bosong Zhang (bosongz@princeton.edu)

Current Affiliation (*): Program in Atmospheric and Oceanic Sciences, Princeton University, Princeton, NJ and NOAA/Geophysical Fluid Dynamics Laboratory, Princeton University, Princeton, NJ

Abstract

A vertically resolved analysis of the budget equation for the spatial variance of moist static energy (MSE) is used to diagnose processes associated with the development of tropical cyclones (TCs) in a high-resolution general circulation model (GCM) under realistic boundary conditions. Previous studies have shown that radiation provides an important feedback which enhances TC development. Here we examine the vertical contributions to this feedback by performing a series of mechanism-denial experiments in which synoptic-scale radiative interactions are suppressed either in the boundary layer or in the free troposphere. Although the boundary layer makes up a much smaller proportion of the atmospheric column than the free troposphere, the two experiments result in similar magnitude of reduction in global TC frequency, indicating that radiative interactions in the boundary layer and those in the free troposphere are of comparable importance in modulating TC frequency. Using instantaneous 6-houly outputs, an explicit computation reveals spatial patterns of the advection term during different TC stages. Instead of damping the spatial variance of MSE as noted in previous idealized studies, the advection term is found to promote the development of TCs. We attribute this result primarily to the explicit calculation of the advection term, however the influence of SST gradients cannot be ruled out. While the vertical component of the advection term is prominent in the middle

troposphere, the horizontal component dominates in the boundary layer. These results provide additional insight of how different physical processes contribute to TC development in GCMs under realistic boundary conditions.

Key Points

- Longwave and shortwave feedbacks contribute oppositely to the development of TCs.
- Radiative feedbacks in the boundary layer have comparable impacts on TC frequency as those in the free troposphere.
- Advection promotes the development of TCs under realistic boundary conditions.

Plain Language Summary

The development of tropical cyclones (TCs) involves interactions between radiation, water vapor and circulation. Previous studies usually use column-integrated variables to quantify physical processes associated with TCs under idealized boundary conditions. However, vertical structures of interactions between variables are key to our understanding of TCs. Also, it remains less clear how different physical processes contribute to the development of TCs in the presence of realistic sea surface temperature gradients. In this study we show vertical structures of variables and their interactions associated with TCs simulated in a TC-permitting atmospheric general circulation model. We find that interactions between longwave radiation and water vapor promote TC development, while interactions between shortwave radiation and water vapor inhibit it. When radiative interactions are partially disabled in the boundary layer or in the free troposphere, the global TC frequency shows comparable magnitude of reduction, indicating that radiative feedbacks in the boundary layer are as important as those in the free troposphere in modulating global TC frequency. Through an explicit computation using 6-hourly model outputs, we find that advection contributes positively to TC development under realistic boundary conditions. These results reveal the spatial structure and the role of different physical processes associated with TCs under realistic boundary conditions.

1 Introduction

In numerical simulations of radiative-convective equilibrium (RCE) without rotation, randomly distributed convection can self-aggregate into organized clusters in the presence of idealized boundary conditions. Organized convective systems involve interactions between radiation, moisture, cloud and circulation. An analysis framework based on a variance budget equation for the column-integrated moist static energy [MSE; (Neelin and Held 1987)] is introduced to understand aggregation-related physical processes (Wing and Emanuel 2014). With interactive radiation, the spatial contrast in radiative cooling induces a secondary low-level circulation that transports energy from dry to moist regions,

which plays an important role in the aggregation process (Bretherton et al. 2005; Muller and Held 2012; Wing and Emanuel 2014; Muller and Bony 2015). In simulations with rotation, organized deep convective systems appear in the form of tropical cyclones (TCs). Based on the variance budget equation for the column-integrated MSE, Wing et al. (2016) showed that the spontaneous development of a tropical cyclone from an initially homogeneous environment is promoted by feedbacks involving radiation and the surface fluxes. Similar results are also found in Muller and Romps (2018) in which cyclogenesis is accelerated in the presence of interactive radiation. Overall, cloud radiative interactions promote the development of TCs (Wu et al. 2021; Ruppert et al. 2020). However, Wing et al. (2016) showed that the advection term, computed as a residual from the variance budget equation, contributes negatively to the development of TCs. Thus, the increase in spatial variance of TC-related MSE is mostly driven by diabatic heating.

In addition to numerical simulations under idealized settings, it is necessary to examine physical processes associated with TCs under realistic boundary conditions. General circulation models (GCMs) are useful tools that can provide long-term, global simulations of the climate system. Early studies showed that low-resolution GCMs can simulate vortices that are similar to TCs (Manabe et al. 1970; Broccoli and Manabe 1990). However, biases are found in different aspects. On one hand, low-resolution GCMs tend to simulate fewer TCs than observations (Camargo 2013). On the other hand, TCs simulated in low-resolution GCMs are found to exhibit weaker intensity but larger size (Walsh et al. 2007; Walsh et al. 2015; Camargo et al. 2020). While horizontal grid spacings do make a difference, the simulation of TCs is found to show dependence on other aspects of model configurations such as convective parameterizations (Murakami et al. 2012; Zhao et al. 2012; Duvel et al. 2017).

With advances in computational power, it is possible to study TCs simulated in high-resolution GCMs (Zhao et al. 2009; Wehner et al. 2015; Murakami et al. 2018; Vecchi et al. 2019). However, simply increasing model resolution does not necessarily improve the simulation of TC climatology. For example, Shaevitz et al. (2014) showed that high-resolution GCMs have trouble in simulating the most intense storms. In addition, while the simulated TC frequency is improved by increasing model resolution, the intensity of the simulated TCs measured by 10-m wind speed remains weak (Roberts et al. 2015). TCs are tightly connected with interactions between radiation, clouds, moisture and circulation. Process-orientated diagnostic can help us better understand how different processes contribute to the development of TCs, which can be used to improve the simulation of TCs in GCMs. By comparing TCs simulated in several high-resolution GCMs, Kim et al. (2018) showed that models with stronger TCs tend to have more diabatic heating near the TC center and a greater spatial contrast in relative humidity and surface latent heat flux between the inner and outer regions of TCs. Furthermore, Wing et al. (2019) applied the column-integrated budget analysis to TCs simulated in high-resolution GCMs and showed that models with more intense TCs have stronger surface flux feedback. These results high-

light the importance of interactions between different variables in modulating TC frequency and intensity in numerical simulations with realistic boundary conditions. However, the column-integrated variance budget equation cannot illustrate vertical structures of interactions between radiation, circulation and other state variables (e.g., water vapor) associated with TCs. Recently, Yao et al. (2020) proposed a vertically resolved (VR) analysis framework in which physical processes associated with convective self-aggregation are quantified at each level individually. In a cloud-resolving model without rotation, they found that the radiative feedback increases the spatial variance of MSE, whereas the surface flux feedback reduces it. However, they showed that the advection term mainly reduces the spatial variance of MSE and inhibits aggregation.

Previous studies mainly do numerical simulations under idealized boundary conditions such as spatially uniform sea surface temperatures (SSTs), in which the impact of SST gradients on the development of TCs is missing. It remains unclear how different physical processes contribute to TC genesis in the presence of realistic SST gradients. In this study, we apply the VR analysis framework to TCs simulated in a high-resolution GCM with realistic boundary conditions. Feedbacks involving radiation, moisture and circulation are quantified both horizontally and vertically during different TC stages. We also do mechanism-denial experiments to compare the relative importance of radiative interactions in the boundary layer with those in the free troposphere to global TC climatology. More importantly, we compute the advection term directly using instantaneous 6-hourly model outputs and discuss its role in the development of TCs.

2 Methods

a. Model and tracking TCs

We use the High-Resolution Atmospheric Model (HiRAM) developed at the Geophysical Fluid Dynamics Laboratory (GFDL). With a horizontal grid spacing of ~50 km, HiRAM can reproduce the observed global TC climatology and interannual variability (Zhao et al. 2009). TCs simulated in HiRAM are identified using the tracker developed by Harris et al. (2016). This method uses instantaneous 6-hourly outputs of sea level pressure, mid-tropospheric temperature, 850 hPa vorticity, and 10-m zonal and meridional winds to track high cyclonic vorticity features. Typically, the high cyclonic vorticity is accompanied with a sea-level pressure minimum, a warm core in the middle troposphere and strong near-surface winds. Here we set the minimum wind speed criterion at 15.3 m s^{-1}, which is based on the suggestions of Walsh et al. (2007) of a threshold 10% below gale force (17 m s^{-1}) for models with ~50 km horizontal grid spacing. In addition, we set the minimum warm core temperature anomaly relative to the surrounding environment at 2.5 K to yield comparable global-mean TC frequency as observations. Main results of this study are not sensitive the modest modifications of the tracking parameters used in this study.

b. The VR framework

MSE (denoted as h) is defined as

$$h = c_p T + gz + L_v q, \#(1)$$

where c_p is the specific heat of dry air, T is the air temperature, g is the gravitational acceleration, z is the height above the surface, L_v is the latent heat of vaporization, q is the specific humidity. The budget for the column-integrated MSE (denoted as $\widehat{h}$) is computed as

$$\frac{\partial \widehat{h}}{\partial t} = THF + R - \nabla_h \bullet \widehat{\vec{v}h}, \#(2)$$

where THF is the surface turbulent heat flux including latent and sensible heat flux, R is net radiation of the atmosphere including both shortwave (SW) and longwave (LW) components, and $\nabla_h \bullet \widehat{\vec{v}h}$ is the horizontal convergence of the column-integrated flux of h. Overall, organized convective systems have greater spatial variance of $\widehat{h}$ than disorganized convection over a limited domain. Wing and Emanuel (2014) introduced the variance budget equation for $\widehat{h}$,

$$\frac{1}{2}\frac{\partial \widehat{h}^2}{\partial t} = \widehat{h} \times THF + \widehat{h} \times R - \widehat{h} \times (\nabla_h \bullet \widehat{\vec{v}h}), \#(3)$$

where $\widehat{h} \times THF$ represents the surface flux feedback, $\widehat{h} \times R$ the radiative feedback, and $-\widehat{h} \times (\nabla_h \bullet \widehat{\vec{v}h})$ the advection term. Given that horizontal temperature gradients are small in the tropics, the spatial variance of h is closely related to that of $L_v q$ (Muller and Romps 2018). In the VR framework, the net radiation of a certain atmospheric layer (denoted as R_i and has units of W m^{-2}, where i is the layer index) can be estimated by radiative cooling rates (denoted as tdt_i and has units of K s^{-1}). Specifically, R_i is computed as

$$R_i = \frac{C_p}{g} \times \mathrm{tdt}_i \times \ p_i, \#(4)$$

where p_i is the pressure thickness of the ith layer (units: Pa). Thereafter, we use $L_v q_i \times R_i$ to represent the radiative feedback for the ith layer of the atmospheric column. Likewise, we can estimate the advection term for the ith layer of the atmospheric column. In the VR framework, we note that the advection term consists of the horizontal component, i.e., $-L_v q_i \times (\frac{\partial(u_i \times L_v q_i)}{\partial x} + \frac{\partial(v_i \times L_v q_i)}{\partial y})$ where u_i and v_i are zonal and meridional wind for the ith layer of the atmospheric column with units of m s^{-1}, and the vertical component, i.e., $-L_v q_i \times \frac{\partial(\omega_i \times L_v q_i)}{\partial p}$ where ω_i is the vertical wind component with units of Pa s^{-1}. However, there is no physical meaning in resolving the vertical dimension of the surface flux feedback. For each variable of the ith layer, we consider a ~10° × 10° box centered on the tracked TCs and anomalies are defined as the difference between the actual value at each grid point and its domain average of the ~10° × 10° box.

c. Experiments

All simulations in this study are performed with prescribed climatological monthly means of sea surface temperatures and sea ice from Hadley Centre Sea Ice and Sea Surface Temperature (HadISST) dataset (Rayner et al. 2003) based on the 20-year period from 1986 to 2005, and a constant atmospheric CO_2 concentration at 1990 levels. We first have a simulation that is integrated for 50 years with default model configuration and fully interactive radiation (referred to as the Control run). Zhang et al. (2021) investigated the role of radiative interactions in the development of TCs by doing mechanism-denial experiments in which the model-generated atmospheric radiative cooling rates are overwritten by their monthly-varying climatological values. We note that the overwriting process in Zhang et al. (2021) is implemented over the entire troposphere. In this study, to assess the relative importance of radiative interactions at different levels of the atmosphere, we perform two mechanism-denial experiments: one simulation has suppressed radiative interactions in the boundary layer but interactive radiation in the free troposphere (referred to as the ClimRadBL run); the other simulation has interactive radiation in the boundary layer but suppressed radiative interactions in the free troposphere (referred to as the ClimRadFT run). Table 1 summarizes these simulations.

3 Results

a. Vertical structure of the radiative feedback

Figure 1 shows vertical cross sections of LW and SW components of $R_i^{'}$ and $L_v q_i^{'}$ averaged azimuthally during different TC stages from the 5-15 m s^{-1} bin to the 35-45 m s^{-1} bin. Positive anomalies of LW radiation dominate the atmospheric column from surface to ~200 hPa, whereas negative anomalies of LW radiation are found within a thin layer in the upper troposphere. In comparison, SW radiation exhibits opposite vertical structures. Atmospheric layers with positive anomalies of LW radiation are coincident with negative anomalies of SW radiation and vice versa. Unlike the vertically varied responses in LW and SW radiation, water vapor exhibits a single-peak profile with positive anomalies mainly found in the lower troposphere.

We further our analyses by investigating vertical structure of interactions between $R_i^{'}$ and $L_v q_i^{'}$. Figure 2 shows LW and SW components of $L_v q_i^{'} \times R_i^{'}$ during different TC stages. Positive (negative) anomalies indicate positive (negative) feedbacks. Due to the importance of boundary layer water vapor in regulating the LW emission to the surface (Kramer et al. 2019), the LW feedback peaks in the lower troposphere. While the LW feedback is positive and promotes the development of TCs, the SW feedback is negative and inhibits it. However, the total radiative feedback is positive because the magnitude of SW feedback is smaller than that of the LW feedback (Figure 3, the bottom row). Overall, these results are consistent with previous studies on TCs simulated in convection-

resolving models (Wu et al. 2021; Wing et al. 2016; Muller and Romps 2018; Ruppert et al. 2020). Although the magnitude of perturbation in SW radiation associated with TCs is small, the SW component of $L_v q_i^{'} \times R_i^{'}$ is negative and inhibits the development of TCs. However, in the column-integrated framework, the SW feedback is almost negligible compared to other terms (Wing et al. 2016; Muller and Romps 2018). Similar results are also found in Zhang et al. (2021). One primary reason is that when we compute the density-weighted vertical integration of SW radiation of the entire atmosphere, opposing changes in SW radiation at different levels tend to even out. As a result, the negative SW feedback, which mostly consists of interactions between negative anomalies of SW radiation but positive anomalies of moisture in the lower troposphere, can be overlooked if we do the vertical integration of individual variables first (Figure 3, the top row). Therefore, the magnitude of the radiative feedback can be affected by the order of computation. The column-integrated framework yields stronger LW feedback than the VR framework (Figure 3). Yao et al. (2020) suggested that the column-integrated framework can inadvertently include the impact of remote forcing, which should be accounted for by the advection term.

b. Relative importance of the radiative feedbacks at different levels

Given the vertically varied contribution of the radiative feedback to the development of TCs (Figure 2), we wonder how global TC climatology will be affected when interactions between radiation and convection are partly suppressed in the atmosphere. Specifically, we compare the role of radiative interactions in the boundary layer with those in the free troposphere. To do that, we examine responses of TCs in the ClimRadFT and ClimRadBL runs introduced in Section 2c. In the present-day climate, Zhang et al. (2021) showed that when radiative interactions are entirely suppressed through the troposphere (referred to as the ClimRad run), the global number of TCs is reduced by ~20% for both category 0-5 and category 1-5 TCs compared to that in the Control run. Here, we add the information retrieved from the ClimRad run for reference.

Figure 4 shows the global number of TCs per year in the Control, ClimRad, ClimRadFT, and ClimRadBL runs. Compared to the Control run, the global number of TCs per year exhibit a reduction as long as radiative interactions are suppressed, which reflects the positive contribution of the radiative feedback to the development of TCs in general. However, the magnitude of reduction varies between these simulations. Overall, the ClimRad run exhibits the most robust reduction. In contrast, the magnitude of reduction in the ClimRadFT and ClimRadBL runs is diminished, indicating that partly suppressing radiative interactions is less effective in reducing global TC frequency than entirely suppressing radiative interactions. More importantly, there is no significant difference in the distributions of the global number of TCs per year between the ClimRadFT and ClimRadBL runs, which means that the impact of radiative interactions in the boundary layer is comparable to those in the free troposphere

on global TC climatology. While the boundary layer is a thin layer, the vertical structure shown in Figure 2 reveals that radiative interactions there are of nearly equal importance as those in the free troposphere, which may explain the similar results in the ClimRadFT and ClimRadBL runs.

c. Role of the advection term

Like previous studies that compute the advection term as a residual in the column-integrated framework (Wing and Emanuel 2014; Holloway and Woolnough 2016; Wing et al. 2016; Wing et al. 2019), we investigate the advection term associated with TCs in a similar way in the Control run. Again, h is estimated by $L_v q$ assuming weak horizontal temperature gradients in the tropics, which gives us the simplified column-integrated variance budget equation:

$$\frac{1}{2}\frac{\partial(L_v\hat{q}^{'})^2}{\partial t} \approx L_v\hat{q}^{'} \times \mathrm{THF}^{'} + L_v\hat{q}^{'} \times \mathrm{LW}^{'} + L_v\hat{q}^{'} \times \mathrm{SW}^{'} + residual. \#(5)$$

The schematic diagram in Figure 5 illustrates how the tendency term ($\frac{1}{2}\frac{\partial(L_v\hat{q}^{'})^2}{\partial t}$) on the left-hand side of Equation 5 is computed: there are three boxes centered on a tracked TC, representing locations A, B and C with time steps at t_0, t_0+6 h and $t_0 + 12$ h, respectively. To compute the tendency term at location B, we use

$$\frac{1}{2}\frac{\left(L_v\hat{q}^{'}\right)^2_{B,\ t_0+6\ h} - \left(L_v\hat{q}^{'}\right)^2_{B,\ t_0}}{t}. \#(6)$$

Here t is 6 h. Figure 6 shows composites of $\frac{1}{2}\frac{\partial(L_v\hat{q}^{'})^2}{\partial t}$, $L_v\hat{q}^{'} \times \mathrm{THF}^{'}$, $L_v\hat{q}^{'} \times \mathrm{LW}^{'}$, $L_v\hat{q}^{'} \times \mathrm{SW}^{'}$ and the residual term during different TC stages. The tendency term has an order of ~1.0×10^{10} J m^{-2}, whereas $L_v\hat{q}^{'} \times \mathrm{THF}^{'}$ and $L_v\hat{q}^{'} \times \mathrm{LW}^{'}$ have an order of ~1.0×10^{9} J m^{-2}. As TCs get stronger, $L_v\hat{q}^{'} \times \mathrm{THF}^{'}$ plays a more important role than $L_v\hat{q}^{'} \times \mathrm{LW}^{'}$. One primary reason is that as TC-related winds become stronger, surface fluxes are enhanced, which forms a positive feedback that promotes the development of TCs. This process is often referred to as a wind-induced surface heat exchange (WISHE) feedback (Emanuel 1986). Similar contribution from the surface flux feedback is also found in RCE simulations with rotation (Wing et al. 2016; Muller and Romps 2018), but may be absent for convective aggregation in simulations without rotation where air-sea enthalpy disequilibrium can overwhelm the surface wind feedback (Wing and Emanuel 2014). On the other hand, while $L_v\hat{q}^{'} \times \mathrm{LW}^{'}$ is positive, $L_v\hat{q}^{'} \times \mathrm{SW}^{'}$ is almost zero during different TC stages. As mentioned in Section 3a, the density-weighted vertical integral of SW radiation alone would smooth out opposing anomalies at different levels, making the SW feedback almost negligible in comparison to the LW feedback (Figure 3, the top row).

With the tendency term and the first three terms on the right-hand side of Equation 5 quantified, we can compute the advection term as a residual. Since $\frac{1}{2}\frac{\partial(L_v\hat{q}^{'})^2}{\partial t}$ is one order of magnitude greater than the surface flux feedback and the radiative feedback, it comes as no surprise that the advection term shows similar magnitude and horizontal patterns as the tendency term: negative anomalies are found in outer regions, whereas positive anomalies are discernable near the TC centers although they do not entirely overlap the positive anomalies of the radiative feedback and the surface flux feedback (Figure 6). However, these results indicate that the advection term is a primary driver of TC-related convection, at least near the TC center. In RCE simulations with rotation, Wing et al. (2016) found that the spatial variance of MSE is mainly driven by diabatic heating but damped by the advection. When it comes to TCs simulated in high-resolution GCMs with realistic boundary conditions, Wing et al. (2019) showed that the advection term is a negative contribution to the development of TCs. However, they pointed out that the advection term computed as a residual may not accurately reflect the impact of advection on TCs.

Therefore, an explicit computation is needed to address the discrepancy in the sign of the advection term. Another advantage of the explicit computation is to show the vertical structure of the advection term, which is missing in the column-integrated framework. Here, we use the model-generated four-dimensional instantaneous 6-hourly outputs to do so. Instead of directly diving into the advection term, we start with the horizontal convergence of the wind field (i.e., $\nabla \bullet \overrightarrow{v_h} = \frac{\partial u}{\partial x} + \frac{\partial v}{\partial y}$), where u and v are zonal and meridional wind respectively. The partial derivatives are computed using centered finite differences. The vertical structure of $[\nabla \bullet \overrightarrow{v_h}]^{'}$ reflects primary features of TCs, with convergence in the boundary layer but divergence in the upper troposphere (Figure 7). Also, the vertical structure of $\left[\frac{\partial \omega}{\partial p}\right]^{'}$ is just the opposite of $[\nabla \bullet \overrightarrow{v_h}]^{'}$ given that mass is conserved (not shown).

In the VR framework, both the horizontal and vertical convergence of the flux of moisture can be quantified. To have the same physical meaning as the radiation and surface fluxes in which positive/negative values means heating/cooling of the atmosphere, we retain the negative signs in front of them and use the two equations listed below:

$$-\left[\nabla \bullet (\overrightarrow{v_h} \times L_v q)\right]^{'} = -\left[\frac{\partial (u \times L_v q)}{\partial x} + \frac{\partial (v \times L_v q)}{\partial y}\right]^{'}, \#(7)$$

$$-\left[\nabla \bullet (\omega \times L_v q)\right]^{'} = -\left[\frac{\partial (\omega \times L_v q)}{\partial p}\right]^{'}. \#(8)$$

For the term in Equation 7, it increases as TCs get stronger with positive values dominate in the boundary layer, indicating strong convergence of moisture into the center of TCs (Figure 8, the top row). In comparison, although the vertical component defined in Equation 8 also increases as TCs get stronger, positive

anomalies are mainly found in the middle troposphere while negative anomalies appear in the boundary layer (Figure 8, the middle row). Overall, both the horizontal and vertical convergence of flux of moisture add heating to the atmospheric column although they work on different regions. We note that the two terms in Figure 8 have the same units of W m^{-2} as LW and SW radiation shown in Figure 1. However, it is noticeable that the magnitude of the convergence of flux is much stronger than that of radiation.

We further our analyses by computing the horizontal and vertical components of the advection term, which are

$$-L_v q^{'} \times \left[\nabla \bullet (\overrightarrow{v_h} \times L_v q)\right]^{'} = -L_v q^{'} \times \left[\tfrac{\partial (u \times L_v q)}{\partial x} + \tfrac{\partial (v \times L_v q)}{\partial y}\right]^{'}, \#(9)$$

$$-L_v q^{'} \times \left[\nabla \bullet (\omega \times L_v q)\right]^{'} = -L_v q^{'} \times \left[\tfrac{\partial (\omega \times L_v q)}{\partial p}\right]^{'}. \#(10)$$

Physically, these two terms represent interactions between MSE and the convergence of MSE in the horizontal and vertical directions, respectively. If positive anomalies of convergence ($-\left[\nabla \bullet (\overrightarrow{v_h} \times L_v q)\right]^{'} > 0$ or $-\left[\nabla \bullet (\omega \times L_v q)\right]^{'} > 0$) are coincident with positive anomalies of $L_v q^{'}$, the advection term will further increase the already positive anomalies of $L_v q^{'}$, which is regarded as a positive feedback. With this in mind, Figure 9 shows the terms defined in Equation 9 and 10. Overall these two terms show similar vertical structures as in Figure 8: both terms increase as TCs get stronger, with positive anomalies of the vertical component mainly found in the middle troposphere while positive anomalies of the horizontal component in the boundary layer. The step-by-step explicit computation reveals that the advection term, including the vertical and horizontal components, plays an important role in enhancing the spatial variance of MSE and thus contributes positively to the development of TCs. Recently, Reyes and Yang (2020) showed that over spatially uniform SSTs, TC genesis can happen without radiative and surface flux feedbacks, which indicates that interactions between circulation and convection help TC genesis. The explicit computation in this study provides evidence that advection contributes positively to TC development. However, we note that the influence of SST gradients can also make a difference, which can be explored in future studies.

Based on the results shown in Figure 9, we can also compute the density-weighted vertical integral of the horizontal and vertical components of the advection term. However, the order of computation also makes a difference here as it does in the computation of the radiative feedback. The density-weighted vertical integral can be applied to: (i) $L_v q^{'}$, $-\left[\nabla \bullet (\overrightarrow{v_h} \times L_v q)\right]^{'}$ and $-\left[\nabla \bullet (\omega \times L_v q)\right]^{'}$ individually first, which is referred to as the VI-first approach; or (ii) $-L_v q^{'} \times \left[\nabla \bullet (\overrightarrow{v_h} \times L_v q)\right]^{'}$ and $-L_v q^{'} \times \left[\nabla \bullet (\omega \times L_v q)\right]^{'}$ directly, which is referred to as the VI-second approach. Figure 10 compares the advection term computed in these two approaches. We note that the results using the VI-first

approach is much stronger than those using the VI-second one, especially when TCs get stronger (with wind speeds greater than 25 m s^{-1}). The greater contribution of the advection term computed using the VI-first approach includes indirect effect of interactions of variables between different levels, which lacks physical meanings as mentioned by Yao et al. (2020).

4. Summary and Discussion

In this study, we show vertical structure of interactions between radiation, circulation and moisture associated with TCs simulated in a high-resolution GCM in the presence of realistic boundary conditions. Interactions between radiation and moisture associated with TCs are prominent in the boundary layer. Although perturbations in SW radiation are negative and inhibit the development of TCs, those in LW radiation are positive and stronger in magnitude, leading to an overall positive radiative feedback that promotes the development of TCs. We compare the role of radiative interactions in the boundary layer with those in the free troposphere in the development of TCs by doing mechanism-denial experiments. Qualitatively, the global TC frequency is reduced in both cases. However, suppressing radiative interactions in the boundary layer yields comparable magnitude of reduction in TC frequency as suppressing radiative interactions in the free troposphere even though the boundary layer accounts for a smaller part of the atmosphere than the free troposphere. These results from the mechanism-denial experiments, consistent with the bottom-heavy structure of interactions between radiation and moisture associated with TCs, highlight the importance of diabatic heating in the boundary layer to the development of TCs.

In addition, we compute the advection term as a residual and find that it is a primary driver for the development of TCs. The positive contribution from the advection term is verified by an explicit computation using instantaneous 6-hourly outputs. Near the TC center, the advection term enhances the spatial variance of MSE, which consists of positive contribution from its vertical component in the middle troposphere and its horizontal component in the boundary layer. These results are somewhat contrary to what previous studies have suggested that the advection term is negative and mainly damps TC-related energy. On one hand, computing the advection term as a residual in the column-integrated framework may inadvertently add remote covariance between variables that lacks explainable physical meanings (Yao et al. 2020). On the other hand, model settings such as spatial resolutions and parameterization could affect the sign of the advection term. More studies on the sign of the advection term are needed in GCMs with higher spatial resolutions. Nonetheless, an explicit computation that resolves the vertical dimension can provide more process-oriented information of physical processes. Future work can apply the VR framework to a broader range of models and observations. These detailed investigation of physical processes from different sources can help improve model simulations of

TCs.

Acknowledgement

HiRAM simulations are performed on the Princeton University Research Computing systems. The data sets produced in this study are available from https://tigress-web.princeton.edu/~bosongz/vertical_structure/. This research was supported by NOAA Awards NA18OAR4310269 and NA18OAR4310418, and Department of Energy Award DE-SC0021333.

References

Bretherton, C. S., P. N. Blossey, and M. Khairoutdinov, 2005: An energy-balance analysis of deep convective self-aggregation above uniform SST. *Journal of the atmospheric sciences*, **62,** 4273-4292.Broccoli, A., and S. Manabe, 1990: Can existing climate models be used to study anthropogenic changes in tropical cyclone climate? *Geophysical research letters*, **17,** 1917-1920.Camargo, S. J., 2013: Global and regional aspects of tropical cyclone activity in the CMIP5 models. *Journal of Climate*, **26,** 9880-9902.Camargo, S. J., and Coauthors, 2020: Characteristics of Model Tropical Cyclone Climatology and the Large-Scale Environment. *Journal of Climate*, **33,** 4463-4487.Duvel, J.-P., S. J. Camargo, and A. H. Sobel, 2017: Role of the convection scheme in modeling initiation and intensification of tropical depressions over the North Atlantic. *Monthly Weather Review*, **145,** 1495-1509.Emanuel, K. A., 1986: An air-sea interaction theory for tropical cyclones. Part I: Steady-state maintenance. *Journal of Atmospheric Sciences*, **43,** 585-605.Harris, L. M., S.-J. Lin, and C. Tu, 2016: High-resolution climate simulations using GFDL HiRAM with a stretched global grid. *Journal of Climate*, **29,** 4293-4314.Holloway, C. E., and S. J. Woolnough, 2016: The sensitivity of convective aggregation to diabatic processes in idealized radiative-convective equilibrium simulations. *Journal of Advances in Modeling Earth Systems*, **8,** 166-195.Kim, D., and Coauthors, 2018: Process-oriented diagnosis of tropical cyclones in high-resolution GCMs. *Journal of Climate*, **31,** 1685-1702.Kramer, R. J., B. J. Soden, and A. G. Pendergrass, 2019: Evaluating Climate Model Simulations of the Radiative Forcing and Radiative Response at Earth's Surface. *Journal of Climate*, **32,** 4089-4102.Manabe, S., J. L. Holloway Jr, and H. M. Stone, 1970: Tropical circulation in a time-integration of a global model of the atmosphere. *Journal of Atmospheric Sciences*, **27,** 580-613.Muller, C., and S. Bony, 2015: What favors convective aggregation and why? *Geophysical Research Letters*, **42,** 5626-5634.Muller, C. J., and I. M. Held, 2012: Detailed investigation of the self-aggregation of convection in cloud-resolving simulations. *Journal of the Atmospheric Sciences*, **69,** 2551-2565.Muller, C. J., and D. M. Romps, 2018: Acceleration of tropical cyclogenesis by self-aggregation feedbacks. *Proceedings of the National Academy of Sciences*, **115,** 2930-2935.Murakami,

H., E. Levin, T. Delworth, R. Gudgel, and P.-C. Hsu, 2018: Dominant effect of relative tropical Atlantic warming on major hurricane occurrence. *Science*, **362,** 794-799.Murakami, H., and Coauthors, 2012: Future changes in tropical cyclone activity projected by the new high-resolution MRI-AGCM. *Journal of Climate*, **25,** 3237-3260.Neelin, J. D., and I. M. Held, 1987: Modeling tropical convergence based on the moist static energy budget. *Monthly Weather Review*, **115,** 3-12.Rayner, N., and Coauthors, 2003: Global analyses of sea surface temperature, sea ice, and night marine air temperature since the late nineteenth century. *Journal of Geophysical Research: Atmospheres*, **108**.Reyes, A. R., and D. Yang, 2020: Spontaneous Cyclogenesis without Radiative and Surface-Flux Feedbacks. *arXiv preprint arXiv:2004.08662*.Roberts, M. J., and Coauthors, 2015: Tropical cyclones in the UPSCALE ensemble of high-resolution global climate models. *Journal of Climate*, **28,** 574-596.Ruppert, J. H., A. A. Wing, X. Tang, and E. L. Duran, 2020: The critical role of cloud–infrared radiation feedback in tropical cyclone development. *Proceedings of the National Academy of Sciences*, **117,** 27884-27892.Shaevitz, D. A., and Coauthors, 2014: Characteristics of tropical cyclones in high-resolution models in the present climate. *Journal of Advances in Modeling Earth Systems*, **6,** 1154-1172.Vecchi, G. A., and Coauthors, 2019: Tropical cyclone sensitivities to CO 2 doubling: roles of atmospheric resolution, synoptic variability and background climate changes. *Climate Dynamics*, **53,** 5999-6033.Walsh, K., M. Fiorino, C. Landsea, and K. McInnes, 2007: Objectively determined resolution-dependent threshold criteria for the detection of tropical cyclones in climate models and reanalyses. *Journal of climate*, **20,** 2307-2314.Walsh, K. J., and Coauthors, 2015: Hurricanes and climate: the US CLIVAR working group on hurricanes. *Bulletin of the American Meteorological Society*, **96,** 997-1017.Wehner, M., K. A. Reed, D. Stone, W. D. Collins, and J. Bacmeister, 2015: Resolution dependence of future tropical cyclone projections of CAM5. 1 in the US CLIVAR Hurricane Working Group idealized configurations. *Journal of Climate*, **28,** 3905-3925.Wing, A. A., and K. A. Emanuel, 2014: Physical mechanisms controlling self-aggregation of convection in idealized numerical modeling simulations. *Journal of Advances in Modeling Earth Systems*, **6,** 59-74.Wing, A. A., S. J. Camargo, and A. H. Sobel, 2016: Role of radiative–convective feedbacks in spontaneous tropical cyclogenesis in idealized numerical simulations. *Journal of the Atmospheric Sciences*, **73,** 2633-2642.Wing, A. A., and Coauthors, 2019: Moist static energy budget analysis of tropical cyclone intensification in high-resolution climate models. *Journal of Climate*, **32,** 6071-6095.Wu, S. N., B. Soden, and D. Nolan: Examining the Role of Cloud Radiative Interactions in Tropical Cyclone Development using Satellite Measurements and WRF Simulations. *Geophysical Research Letters*, e2021GL093259.Yao, L., D. Yang, and Z.-M. Tan, 2020: A Vertically Resolved MSE Framework Highlights the Role of the Boundary Layer in Convective Self-Aggregation. *arXiv preprint arXiv:2008.10158*.Zhang, B., B. J. Soden, G. A. Vecchi, and W. Yang, 2021: The role of radiative interactions in tropical cyclone development under realistic boundary conditions. *Journal of Climate*, **34,** 2079-2091.Zhao, M., I. M. Held, and S.-J. Lin, 2012: Some counterintuitive dependencies of tropical cyclone frequency on parameters in a GCM. *Journal of*

the Atmospheric Sciences, **69,** 2272-2283.Zhao, M., I. M. Held, S.-J. Lin, and G. A. Vecchi, 2009: Simulations of global hurricane climatology, interannual variability, and response to global warming using a 50-km resolution GCM. *Journal of Climate*, **22,** 6653-6678.

Tables

Table 1 A list of the simulations conducted in this study.

Experiment name	SST forcing	CO_2 forcing	Radiation
Control	1986-2005 Average	Fixed	Fully Interactive
ClimRadFT	1986-2005 Average	Fixed	Prescribed Climatology in the Free Troposphere; Full
ClimRadBL	1986-2005 Average	Fixed	Prescribed Climatology in the Boundary Layer; Fully

Figures

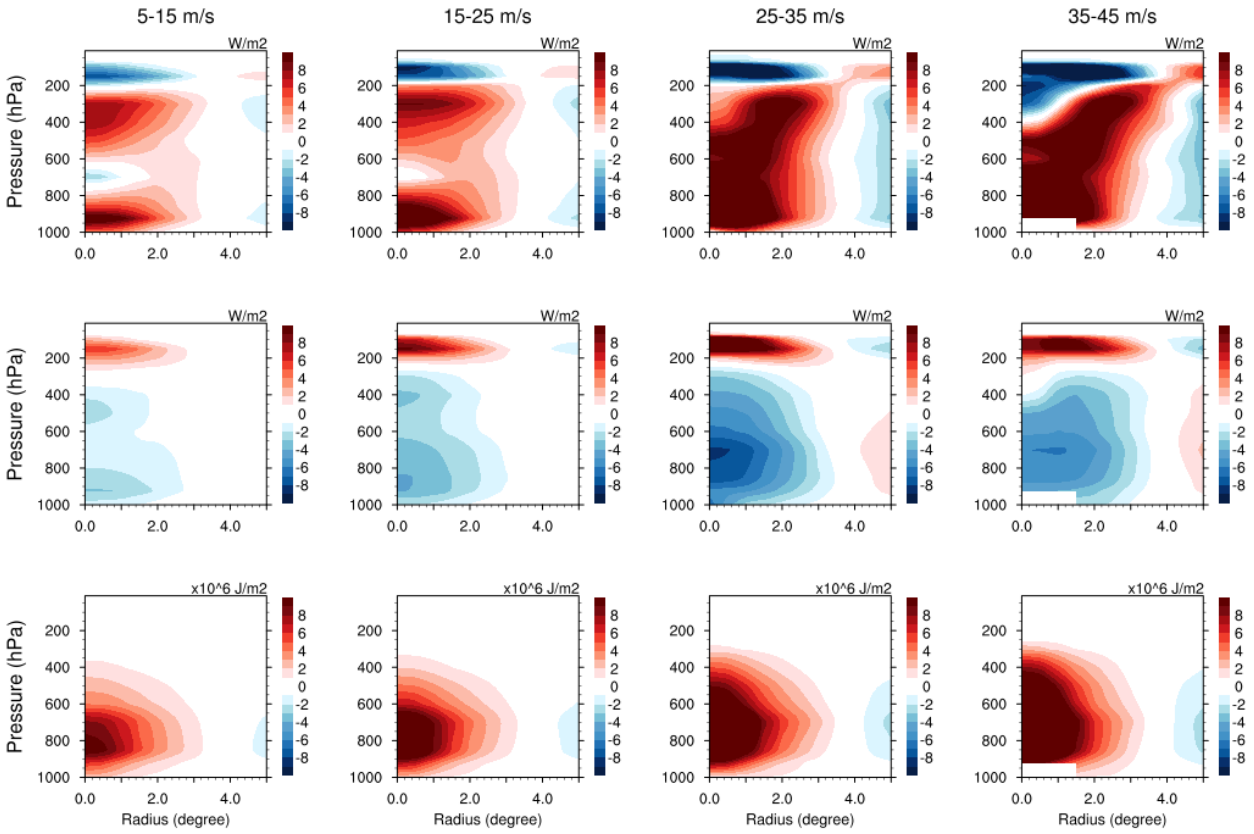

Figure 1 Vertical cross sections of azimuthally averaged and density-weighted LW component of $R_i^{'}$ (top), SW component of $R_i^{'}$ (mid) with units of W m^{-2}, and $L_v q^{'}$ (bottom) with units of 1×10^6 J m^{-2} during different TC stages: 5-15 m s^{-1}, 15-25 m s^{-1}, 25-35 m s^{-1} and 35-45 m s^{-1} (from left to right).

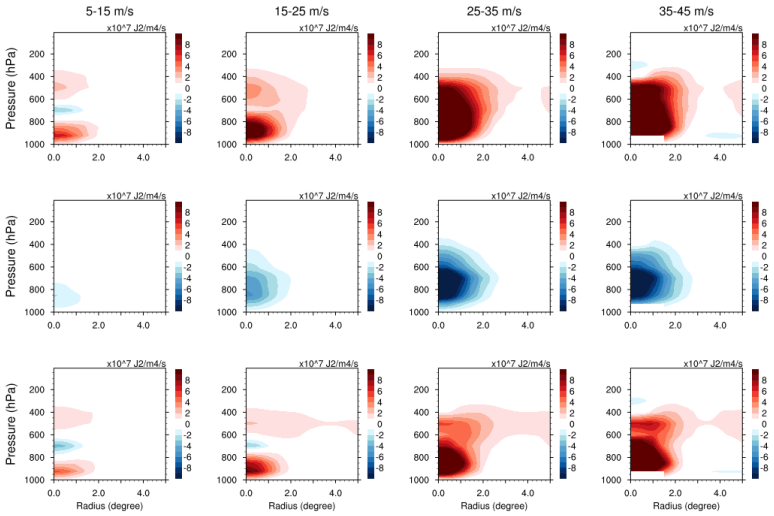

Figure 2 Same as Figure 1 but for LW component (top) and SW component (bottom) of $L_v q_i^{'} \times R_i^{'}$ with units of 1×10^7 J^2 m^{-4} s^{-1}.

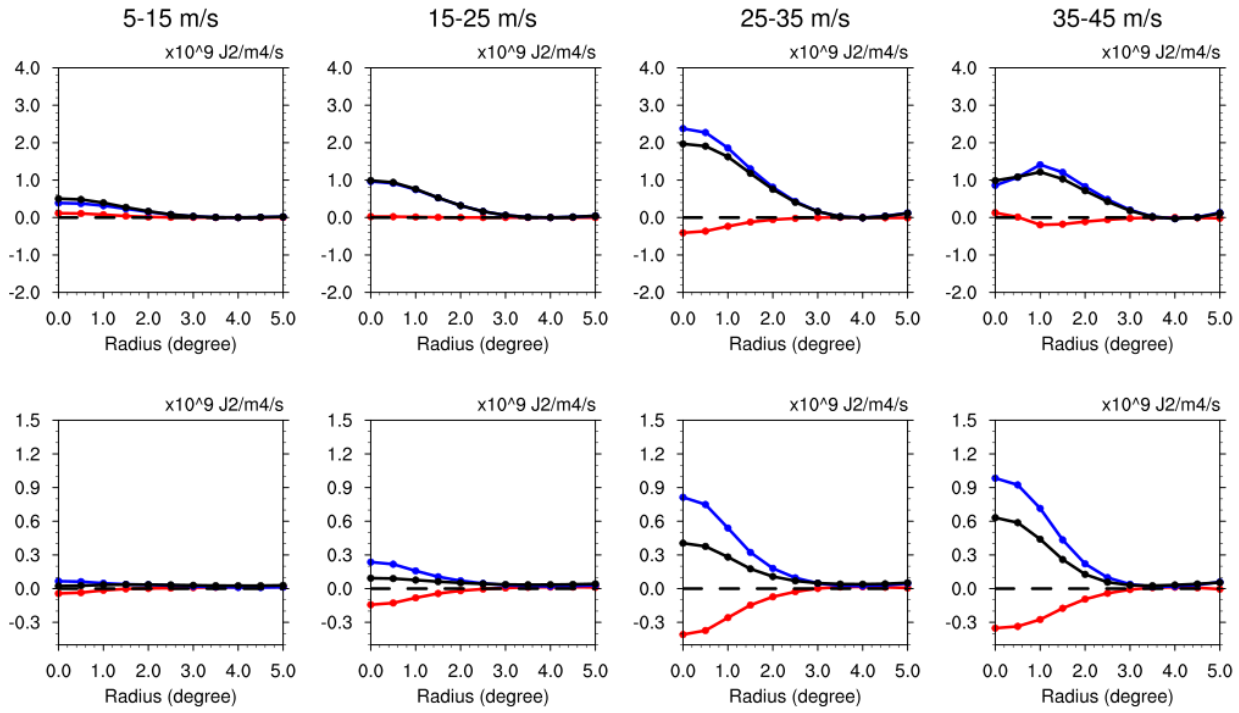

Figure 3 Azimuthal average of composites of the SW (red lines), LW (blue lines) and total (black lines) radiative feedbacks computed in the column-integrated framework (top row), and in the VR framework with density-weighted vertical integral applied to each component (bottom row). The vertical integration is done between 850 hPa and 100 hPa.

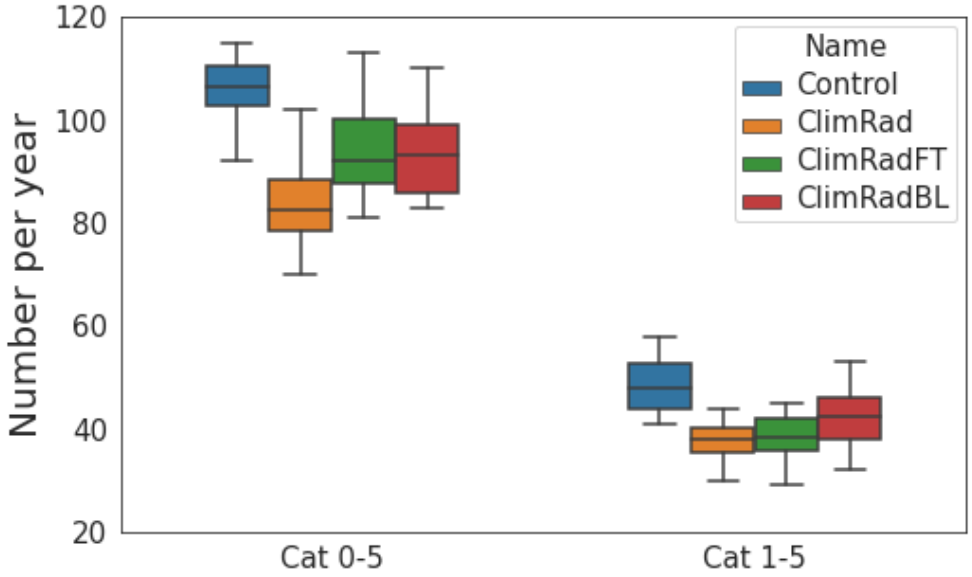

Figure 4 Boxplots of the global number of TCs per year for category 0-5 and category 1-5 TCs for the Control run (blue), ClimRad run (orange), ClimRadFT run (green), and ClimRadBL run (red).

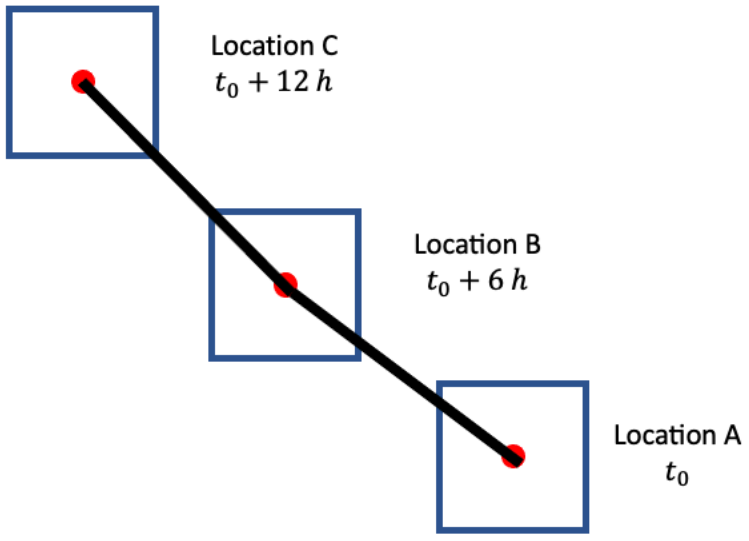

Figure 5 A schematic diagram showing three boxes centered on a tracked TC with locations A, B and C and time steps t_0, $t_0 + 6\ h$ and $t_0 + 12\ h$, respectively.

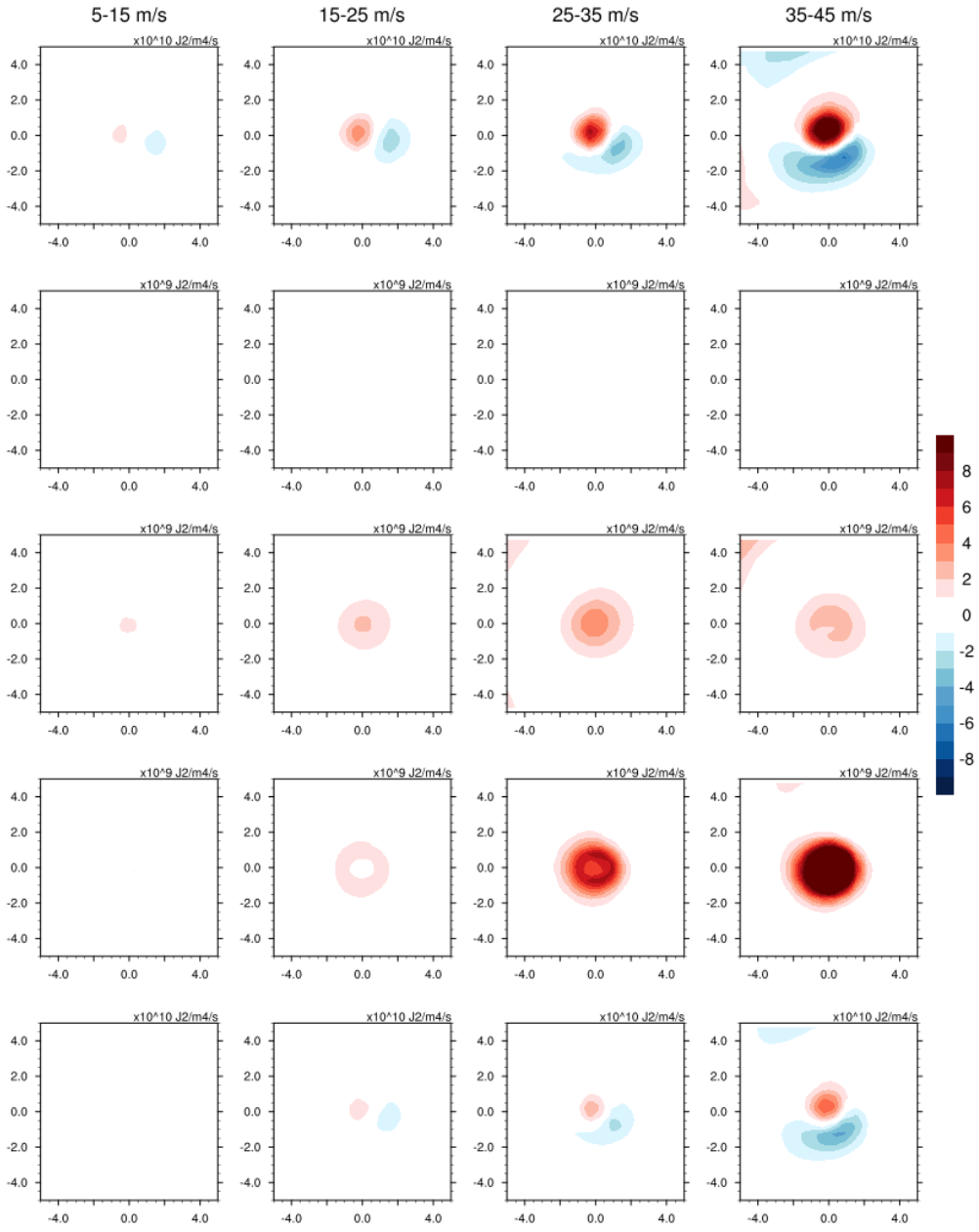

Figure 6 Composites of $\frac{1}{2}\frac{\partial(L_v\hat{q}^{'})^2}{\partial t}$ (top row; 1×10^{10} J^2 m^{-4} s^{-1}), $L_v\hat{q}^{'} \times \mathrm{SW}^{'}$ (second row; 1×10^{9} J^2 m^{-4} s^{-1}), $L_v\hat{q}^{'} \times \mathrm{LW}^{'}$ (third row; 1×10^{9} J^2 m^{-4} s^{-1}), $L_v\hat{q}^{'} \times \mathrm{THF}^{'}$ (fourth row; 1×10^{9} J^2 m^{-4} s^{-1}), and the residual term (bottom row; 1×10^{10} J^2 m^{-4} s^{-1}) during different TC stages: 5-15 m s^{-1}, 15-25 m s^{-1}, 25-35 m s^{-1} and 35-45 m s^{-1} (from left to right).

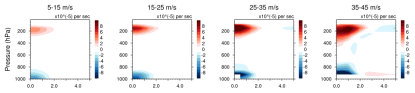

Figure 7 Same as Figure 1 but for the horizontal convergence of the wind field ($[\nabla \bullet \overrightarrow{v_h}]'$) with units of 1×10^{-5} s^{-1}.

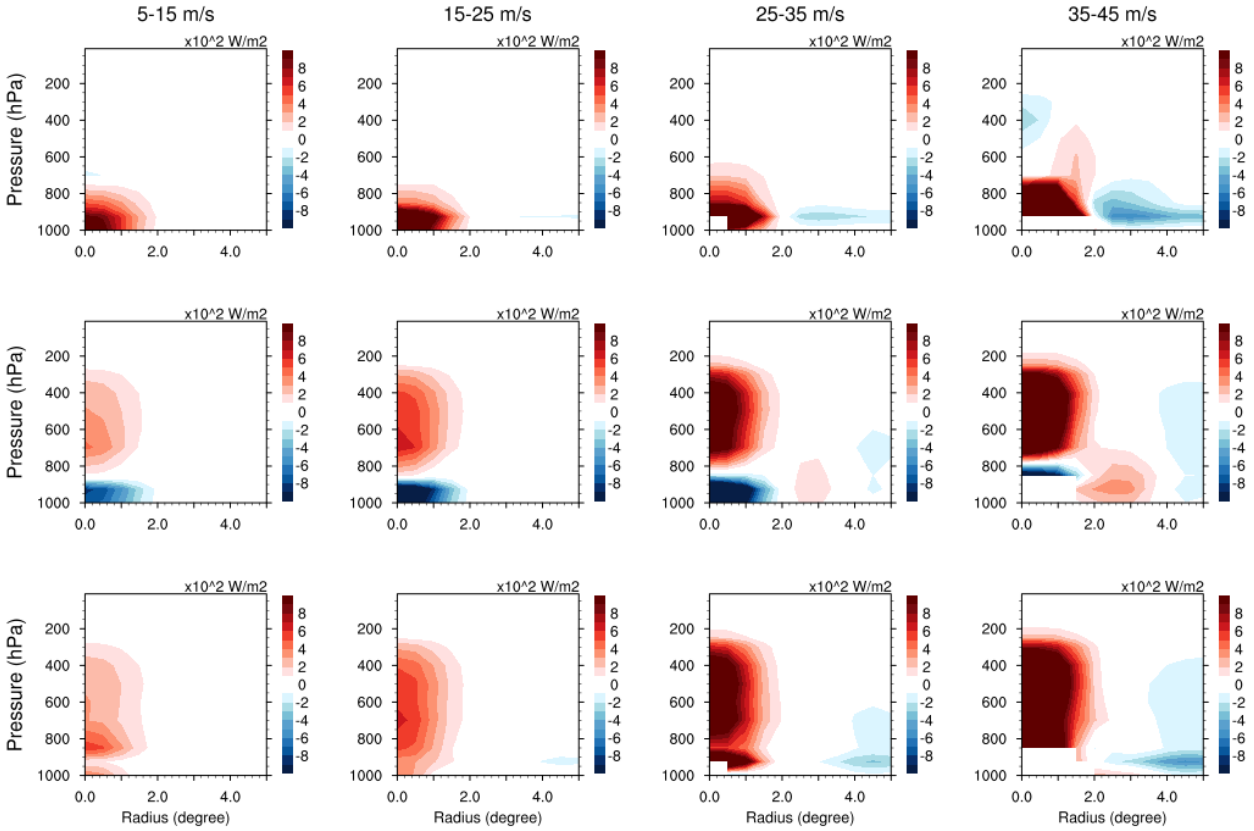

Figure 8 Same as Figure 1 but for $-\left[\nabla \bullet (\overrightarrow{v_h} \times L_v q)\right]'$ (top) and $-\left[\nabla \bullet (\omega \times L_v q)\right]'$ (middle) and the sum of them (bottom) with units of 1×10^2 W m^{-2}.

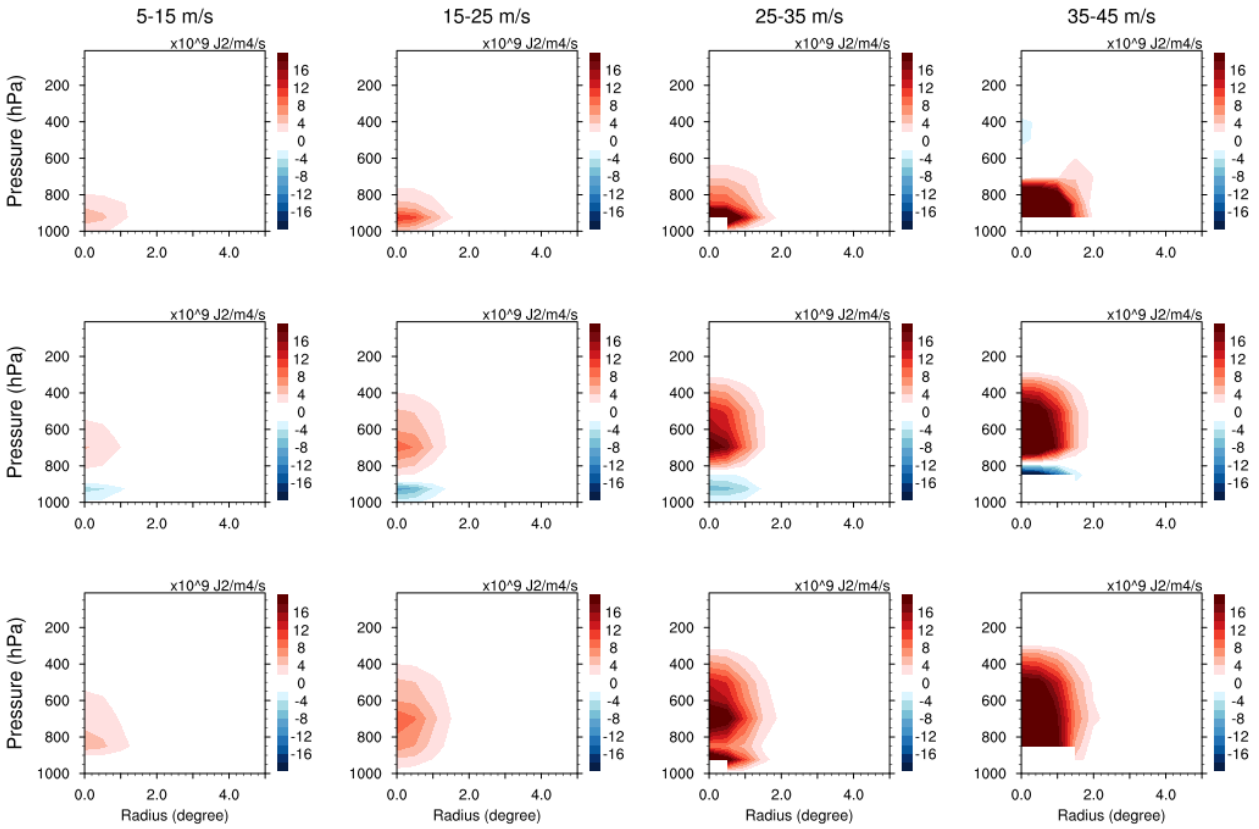

Figure 9 Same as Figure 1 but for $-L_v q^{'} \times [\nabla \bullet (\overrightarrow{v_h} \times L_v q)]^{'}$ (top), $-L_v q^{'} \times [\nabla \bullet (\omega \times L_v q)]^{'}$ (middle) and the sum of them (bottom) with units of 1×10^9 J^2 m^{-4} s^{-1}.

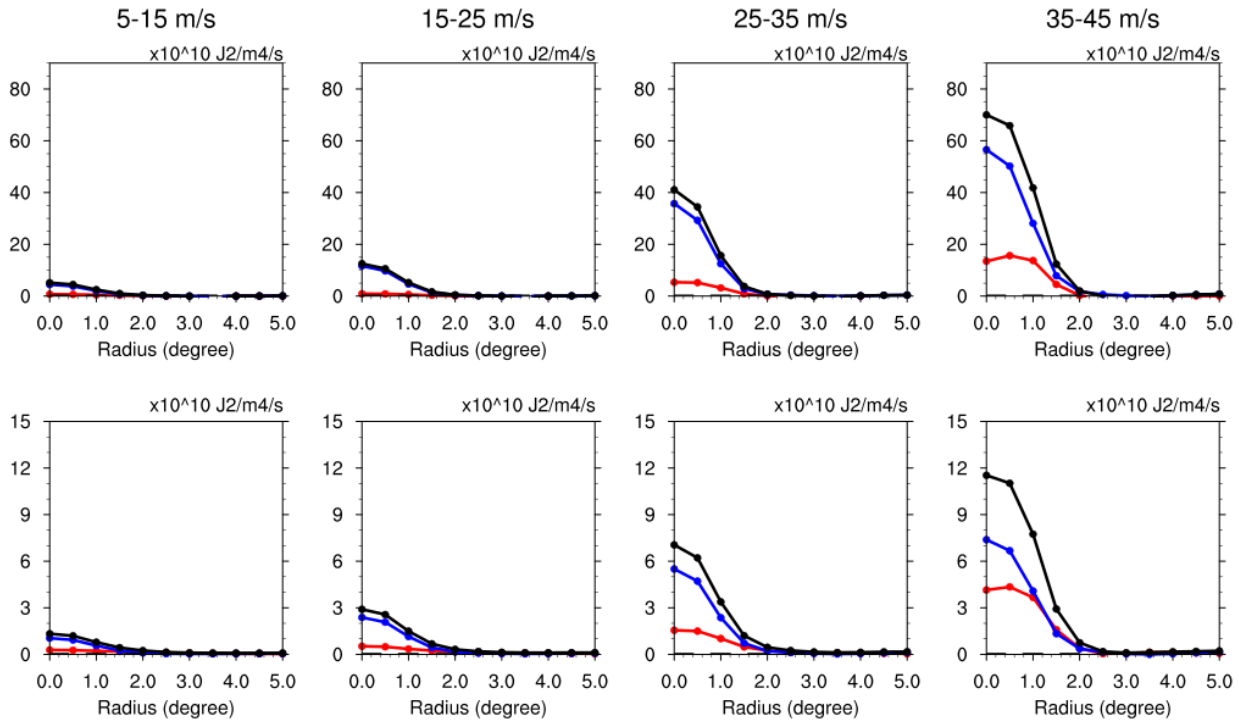

Figure 10 Azimuthal mean of composite of the horizontal (red lines) and vertical (blue lines) components of the advection term computed by the VI-first approach (top row) and by the VI-second approach (bottom row) with units of 1×10^{10} J^2 m^{-4} s^{-1}. The black lines represent the sum of the horizontal and vertical components. Vertical integration is done between 850 hPa and 100 hPa.